Relationship between Low Stratiform Cloud Amount and Estimated Inversion Strength in the Lower Troposphere over the Global Ocean in Terms of Cloud Types

Koshiro, Tsuyoshi; Shiotani, Masato

Journal of the Meteorological Society of Japan, Vol. 92, No. 1, pp. 107–120, 2014
DOI:10.2151/jmsj.2014-107

Relationship between Low Stratiform Cloud Amount and Estimated Inversion Strength in the Lower Troposphere over the Global Ocean in Terms of Cloud Types

Tsuyoshi KOSHIRO and Masato SHIOTANI

Research Institute for Sustainable Humanosphere, Kyoto University, Kyoto, Japan

(Manuscript received 27 June 2013, in final form 27 October 2013)

Abstract

Low stratiform clouds (LSCs) are of three different types: stratocumulus (Sc), stratus (St), and sky-obscuring fog (FOG). Ship-based cloud observations (September 1957–August 2002) and air-temperature and sea-level pressure data obtained from the ERA-40 reanalysis are used to investigate the seasonal relationships between the amounts of these LSC types and the estimated inversion strength (EIS) over the global ocean. Although it is known that a single linear relationship applies to the variations in the LSC amount as the sum of those of the LSC types and EIS, two relationships with different sensitivities are found between each LSC-type amount and EIS. The boundary lies at a sea surface temperature (SST) of approximately 16°C. The Sc amount is strongly correlated with EIS in the warm SST regime, whereas no correlation can be observed between them in the cold SST regime. In contrast, although FOG rarely occurs in the warm SST regime, its amount increases with EIS in the cold SST regime. The St amount increases with EIS in both regimes, with higher sensitivity in the cold SST regime. Examination of vertical layers contributing to EIS reveals that an increase in the inferred inversion strength between 850- and 925-hPa levels corresponds to that in the Sc amount in the warm SST regime. In the cold SST regime, as EIS increases, relatively high values of inferred inversion strength between 700- and 850-hPa levels change to a rapid increase in that between 925-hPa level and the surface, which coincides with the transition from Sc to FOG. Temperature advection implied by the air–sea temperature difference provides favorable conditions to the different variations in the two regimes: general occurrence of cold advection in the warm SST regime and cold-to-warm transition of advection in the cold SST regime.

Keywords low stratiform cloud; inversion strength; sea surface temperature; air–sea temperature difference; temperature advection

1. Introduction

Clouds strongly affect the earth's climate by influencing the radiation budget. Low stratiform clouds (LSCs), which are primarily found over the ocean, are especially important because of their high albedos relative to the surface and cloud-top temperatures close to those of the surface that can greatly reduce the net radiation at the top of the atmosphere (e.g., Ramanathan et al. 1989; Harrison et al. 1990; Hartmann et al. 1992). Therefore, it is important to understand the factors controlling the LSC amount over the global ocean.

For a global perspective, previous studies have mainly focused on seasonal to interannual variability of the LSC amount and its relationship to other climate parameters (e.g., Klein and Hartmann 1993; Norris and Leovy 1994; Park and Leovy 2004), although the variability on shorter time scales is also important and has been investigated (e.g., Klein 1997; Xu et al. 2005; George and Wood 2010; Kubar et al. 2012). As is well known, Klein and Hartmann (1993, hereafter KH93) found that seasonal variations in the LSC amount are

Corresponding author and present affiliation: Tsuyoshi Koshiro, Climate Research Department, Meteorological Research Institute, 1-1 Nagamine, Tsukuba, Ibaraki 305-0052, Japan
E-mail: tkoshiro@mri-jma.go.jp

Table 1. The 10 LSC regions defined by KH93. In this study, their five subtropical and three midlatitude marine LSC regions are considered, whose abbreviations are represented by one or two alphabetic characters in parentheses.

Region	Location
Subtropical marine LSC regions	
Peruvian (P)	10°–20°S, 80°–90°W
Namibian (N)	10°–20°S, 0°–10°E
Californian (CA)	20°–30°N, 120°–130°W
Australian (A)	25°–35°S, 95°–105°E
Canary Islands (CI)	15°–25°N, 25°–35°W
Midlatitude marine LSC regions	
North Pacic (NP)	40°–50°N, 170°–180°E
North Atlantic (NA)	50°–60°N, 35°–45°W
Circumpolar Ocean (CO)	50°–65°S*
Arctic	80°–90°N
China	20°–30°N, 105°–120°E

* In this study, the geographical extent is indeed 50°–60°S and the JJA season is not considered due to insufficient numbers of ship-based observations.

associated with the lower-tropospheric stability (LTS), which is employed as a measure of temperature inversion strength, defined as the difference between the potential temperatures at 700-hPa level, a sufficiently higher level than the top of the marine boundary layer (MBL), and the surface. As shown in Table 1, they defined 10 regions where LSCs are dominant on the basis of surface-based cloud climatologies by Warren et al. (1986, 1988). They showed that the annual cycle of LSC amounts coincides with that of LTSs in all regions except the Arctic, and a single linear relationship applies for the seasonal variations in the subtropical regions.

Recently, Wood and Bretherton (2006, hereafter WB06) indicated that LTS includes an increase in potential temperature following the mean lapse rate in the lower troposphere, which generally approximates the moist adiabat, and proposed the subtraction of this term from LTS as a new formulation to directly estimate the inversion strength; it is called the estimated inversion strength (EIS). They performed a linear regression analysis similar to that in KH93 using EIS instead of LTS and found that a single linear relationship between the LSC amounts and EISs can apply not only for the LSC regions in the subtropics but also for those in the midlatitudes.

However, "LSCs" is a broad category of clouds, consisting of three types: stratocumulus (Sc), stratus (St), and sky-obscuring fog (FOG). According to the definitions by the World Meteorological Organization (WMO), both Sc and St occur below about 2 km, and they are distinguished by their general shape and structure (WMO 1975): Sc is a patch, sheet, or layer of clouds comprising tessellation, rounded masses, or rolls. St is a cloud layer with a fairly uniform base. FOG is observed as present weather when it is impossible to report cloud type because the sky is obscured by grounded clouds (WMO 1995); it can be considered as an additional LSC type. The relationships between each LSC-type amount and the inferred inversion strength such as EIS have not been demonstrated.

On the other hand, using long-term soundings at several ocean weather stations, Norris (1998a) presented the composite potential temperature profiles for which the same low cloud condition had been reported: Sc typically occurred in a well-mixed MBL under a capping inversion, as observed by many field campaigns in the subtropical oceans (e.g., Albrecht et al. 1988; Lenschow et al. 1988; Albrecht et al. 1995a; Stevens et al. 2003; Bretherton et al. 2004, 2010); St occurred with a moderate stable condition throughout the MBL or in a very shallow layer near the surface; and FOG often occurred with a surface-based inversion. These results imply the existence of temperature inversions at the heights consistent with the morphology of each LSC type. Therefore, it is important to extend the analysis to the global ocean areas. Since EIS only has information about gross strength of temperature inver-

sion between the surface and the 700-hPa level, it is required to define new measures indicating the inversion strengths for several vertical levels within the lower troposphere.

In addition, to identify processes responsible for different LSC types, several studies have focused on advection over the sea surface temperature (SST) gradient. In the subtropical eastern Pacific, an increase in the LSC amount, most of which are Sc, is associated with cold advection (Klein et al. 1995; Klein 1997; Xu et al. 2005; Mansbach and Norris 2007). In contrast, FOG typically forms with warm advection over the cold ocean in the midlatitudes (Norris and Klein 2000; Tokinaga and Xie 2009). Moreover, across the strong SST fronts in the North Pacific during the summer, changes in wind direction over the SST gradient cause a cloud regime transition between Sc or St and FOG (Norris and Iacobellis 2005; Tanimoto et al. 2009). These effects of synoptic temperature advection are supposed to be reflected in the relationships between the LSC-type amounts and the inferred inversion strength.

For these investigations, satellite cloud data such as the International Satellite Cloud Climatology Project (ISCCP) products (Rossow and Schiffer 1999) as well as the ship-based observations are available. In recent years, the "A-Train" satellite observations, including active sensor measurements, have been intensively investigated in terms of the amount and other properties of LSCs (e.g., Jensen et al. 2008; Lin et al. 2009; Zhang et al. 2009; Yue et al. 2011; Huang et al. 2012; Kubar et al. 2012). However, in regions with large amounts of higher level clouds, LSCs observed from satellites can be obscured by them, especially by using passive sensors (e.g., Weare 1999, 2000). Furthermore, the definitions of cloud types are different for human observations from the surface and satellite observations (e.g., Hahn et al. 2001; Sassen and Wang 2008). Therefore, for a global analysis of the LSC-type amounts, long-term ship-based observations are suitable and still important, even though the resolution decreases due to the sparseness of spatial and temporal sampling.

In this paper, using the ship-based cloud report archive, we demonstrate relationships between the amount of each LSC type (Sc, St, and FOG) and the inversion strength in the lower troposphere measured by EIS over the global ocean. Details of the data used in this study are described in Section 2. In Section 3, we present the relationships for each LSC type. These relationships are sorted out by SST, and warm and cold SST regimes are defined. For the two regimes, we examine the correspondence of the inferred inversion strengths for three vertical levels within the lower troposphere that we introduce and temperature advection implied by the air–sea temperature difference with the relationships. Conclusions are given in Section 4.

2. Data

2.1 Cloud amount

The cloud amount was calculated from the ship-based data of the Extended Edited Cloud Report Archive (EECRA, Hahn and Warren 2009; Eastman et al. 2011), which is a collection of individual synoptic surface observations for cloud properties obtained from the Comprehensive Ocean-Atmosphere Data Set (COADS, Woodruff et al. 1987, 1998). The EECRA defines 12 low cloud condition codes (C_L): 10 regular codes in accordance with the WMO synoptic codes (WMO 1995) and 2 extended codes for obscured sky conditions. Each report contains C_L and a low cloud amount at a certain time and place.

This study considered three types of LSCs: Sc (C_L = 4, 5, 8), St (C_L = 6), and FOG (C_L = 11). The LSCs correspond to the sum of three types: C_L = 4, 5, 6, 8, 11. The code C_L = 7 also indicates St in EECRA; however, from its definition, this cloud type is often observed in association with nimbostratus and deep convective clouds. In these cases, because the MBL properties are related to the deeper clouds rather than LSCs, only codes C_L = 6 were used as St.

We constructed the 5° × 5° seasonal climatologies of the Sc, St, FOG, and LSC amounts from September 1957 to August 2002, according to the computational methods described in the EECRA documentation, which are based on the algorithm used in Warren et al. (1986, 1988) and Norris (1998b). Basically, the time-averaged amount of a cloud type can be obtained as the product of frequency-of-occurrence (fraction of weather observations in which a cloud of this type is present) and amount-when-present (average fraction of the sky covered by this cloud type when present). The seasons were defined as follows: December–January–February (DJF), March–April–May (MAM), June–July–August (JJA), and September–October–November (SON). For each season, grid boxes with less than 100 observations contributing to the average were discarded to reduce the sampling error below 3% (Warren et al. 1988). Because most omitted grid boxes are in the high latitudes, the data between 60°N and 60°S were used.

In particular, only daytime [including twilight; defined as the duration when the sun is no more than 9° below the horizon (Hahn et al. 1995)] observations were used to construct the climatologies, because it is difficult for surface observers to identify the low cloud

condition on nights with poor illumination (Hahn et al. 1995; Rozendaal et al. 1995; Norris 1998a). The maxima and minima in the low cloud amount over the ocean typically occur in the early morning and afternoon, respectively (e.g., Minnis et al. 1992; Bretherton et al. 1995; Rozendaal et al. 1995; Bretherton et al. 2004). Cloud liquid water paths retrieved from satellite-based passive microwave observations also tend to show maxima in the early morning and minima in the afternoon over the ocean (e.g., Zuidema and Hartmann 1995; Wood et al. 2002; O'Dell et al. 2008). Because the daytime average includes the diurnal maxima and minima, it may not be very different from the true daily average, as Norris (1998b) pointed out.

2.2 *EIS, SST, and air–sea temperature difference*

EIS was calculated from the following formula given by WB06:

$$\mathrm{EIS} = \left(\theta_{700} - \theta_{\mathrm{sfc}}\right) - \Gamma_{\mathrm{m}}^{850}\left(z_{700} - z_{\mathrm{LCL}}\right), \qquad (1)$$

where θ_{700} and θ_{sfc} are the potential temperatures at the 700-hPa level and the surface, respectively, $\Gamma_{\mathrm{m}}^{850}$ is the moist adiabatic lapse rate at 850-hPa level, z_{700} is the height of the 700-hPa level, and z_{LCL} is the lifting condensation level. As described in WB06, $\Gamma_{\mathrm{m}}^{850}$ was calculated using the mean of the surface and 700-hPa temperatures, and z_{700} was calculated assuming an exponential decrease in pressure with height for a single scale height. z_{LCL} was calculated from the dry adiabat and the lifting condensation temperature estimated by Bolton (1980), with the surface relative humidity fixed at 0.8 following the assumption of WB06. Thus, EIS can be calculated from only the surface pressure and temperatures at the surface and the 700-hPa level. In this study, we used the sea-level pressure, 2-m temperature, and 700-hPa temperature data obtained from the monthly means of the European Centre for Medium-Range Weather Forecasts (ECMWF) 40-year reanalysis (ERA-40, Uppala et al. 2005). The 5° × 5° seasonal climatologies for the full-time period (from September 1957 to August 2002) were constructed from the calculated 2.5° × 2.5° monthly EIS data; only the ocean grid points were considered.

For the same period as ERA-40, SST data were taken from the Hadley Centre sea ice and sea surface temperature data set (HadISST) version 1.1 (Rayner et al. 2003) and were averaged to obtain the 5° × 5° seasonal climatologies, as the original data are 1° × 1° monthly means. Only the 5° × 5° grid boxes where sea ice does not exist were considered.

The SST data were also used to construct the 5° × 5° seasonal climatologies of air–sea temperature difference with the 2-m temperature data from ERA-40. The air–sea temperature difference, which is often employed as a measure of near-surface atmospheric stability (e.g., Park and Leovy 2004; Tokinaga and Xie 2009), reflects the synoptic advection over the ocean for longer time means such as seasonal climatologies; a positive value corresponds to average warm advection, while a negative value to average cold advection.

3. Results

3.1 *Relationships between the LSC-type amounts and EIS*

First, we confirm the relationship between seasonal climatologies of the LSC amount and those of EIS over the global ocean. Figure 1 displays a frequency distribution obtained by classifying each 5° × 5° climatological seasonal value into 0.5 K intervals of EIS and 2.5% intervals of the LSC amount. A scatter plot only for KH93's LSC regions is also shown. As demonstrated by WB06 including the Chinese region and using other reanalysis data to calculate EIS, the scatter plot indicates a single linear relationship for both the subtropical (red open markers) and the midlatitude (blue filled markers) regions. The result for the global ocean areas is quite similar to only that for KH93's LSC regions; there is a clear positive correlation between the LSC amount and EIS, with a correlation coefficient of 0.87, although the occurrence is less frequent as EIS increases. A linear regression analysis indicates that the LSC amounts increase by 4.7% per 1 K increase in EIS. Hence, the seasonal relationship between the LSC amount and EIS is almost universal; that is, a single linear relationship can be applied not only to the selected LSC regions but also to the global ocean areas including those with small LSC amounts.

Next, we divide the LSC amount into three types. Figure 2 shows the same distributions as Fig. 1, except for the amounts of Sc, St, and FOG. Focusing first on the scatter plots for the LSC regions defined by KH93, it is found that the relationships between the subtropical (red open markers) and midlatitude (blue filled markers) regions are different. In Fig. 2a, the Sc amounts are strongly correlated with EISs in the subtropical regions, whereas they are approximately 30% regardless of EIS in the midlatitude regions. In Fig. 2b, the St amounts show positive correlations with EISs in both the subtropical and midlatitude regions, with higher sensitivity in the midlatitudes, although they are generally smaller than the Sc amounts. In Fig. 2c, FOG is rarely observed in the subtropics; however, FOG amounts are correlated with EISs in the midlatitude regions.

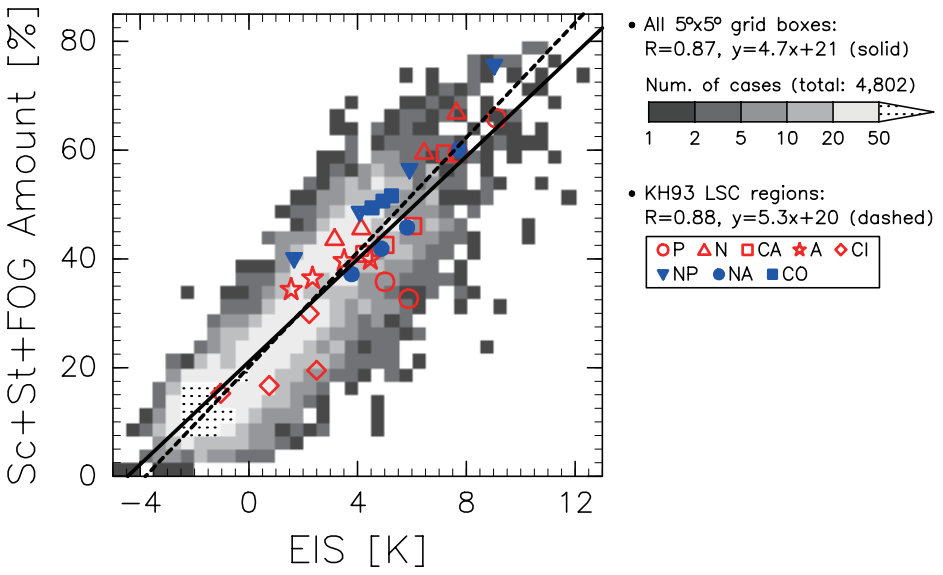

Fig. 1. Frequency of occurrence for EIS and LSC amount intervals for all 5° × 5° seasonal climatologies. The linear regression line is indicated by a solid line. Markers represent a scatter plot of the LSC amount with EIS seasonally averaged for LSC regions defined by KH93 (Table 1); red open and blue filled markers correspond to those in the subtropical and midlatitude oceans, respectively. The linear regression line for the scatter plot is indicated by a dashed line.

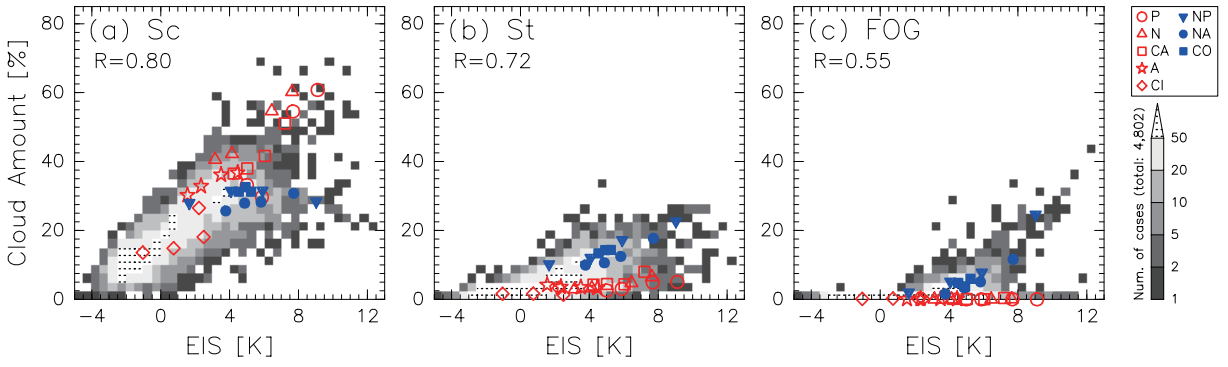

Fig. 2. Similar to Fig. 1 but for (a) Sc, (b) St, and (c) FOG amounts.

The main characteristic features of the distributions for the global ocean areas are quite similar to those for KH93's LSC regions. In Fig. 2a, while the Sc amount is generally larger and its correlation with EIS more clearly seen than other types, the distribution branches off into two domains as EIS increases: one is where the Sc amount increases with EIS, extending from the domain where EISs are negative; the other is where the Sc amounts are approximately 30%, regardless of EIS. The former coincides with the scatter plot for the subtropical regions and the latter with that for the midlatitude regions. Figure 2b shows that the distribution of the St amount also becomes broader with EIS. Even though it is not very clear because of the lower sensitivity, the distribution tends to branch into two relationships, with relatively high sensitivity in a domain corresponding to the midlatitude regions than that to the subtropical regions. On the other hand, as seen in Fig. 2c, the correlation between the FOG amount and EIS is rather unclear, because the occurrence is concentrated where FOG amounts are less than 2.5%. This coincides with the rare occurrence of FOG in the subtropics. However, the FOG amount obviously increases with EIS in other domains, corresponding to

the midlatitude regions. Thus, over the global ocean areas, two relationships with different sensitivities are found between each LSC-type amount and EIS, and they correspond to subtropical and midlatitude regions.

The latitudinal difference shown in Fig. 2 is expected to relate closely to SST, because it primarily decreases with increasing latitude and plays an essential role in regulating the temperature and moisture structures in the lower troposphere. Figure 3 demonstrates in the upper panels the Sc, St, and FOG amounts averaged at 2°C intervals of SST and at 1 K intervals of EIS for all 5° × 5° seasonal climatologies. The results are displayed for the SST range from 2°C to 28°C, because the frequencies and variations of EIS and LSC-type amounts are very small outside this range. The upper panels of Fig. 3 reveal that the distributions of the LSC-type amounts drastically change at an SST of approximately 16°C. As shown in the scatter plots, the KH93's LSC regions in the subtropical and midlatitude oceans are included in the warm and cold SST regimes, respectively. The lower panels of Fig. 3 show that the two relationships for each LSC-type amount observed in Fig. 2 are clearly separated into those in the two regimes.

As shown in the right-hand side of Fig. 3a, the Sc amount significantly increases with EIS in the warm SST regime. Moreover, on average, the Sc amount and EIS increase as SST decreases, although their variances also increase. Therefore, the three variations link together in this regime: an increase in the Sc amount, an increase in EIS, and a decrease in SST. In the cold SST regime (left-hand sides of Figs. 3a–c), although the Sc amounts are the highest among the three types, they are generally approximately 30% regardless of EIS with a slight decrease in higher EISs. Instead, the St and FOG amounts increase with EIS. The maxima in the St and FOG amounts occur in domains where EISs are approximately 10 K and 12 K, respectively, although the occurrence is less frequent with higher EISs. In contrast to the warm SST regime, these variations have little dependence on SST.

Consequently, an SST of 16°C is also the boundary of SST dependence of EIS and the LSC-type amounts. The warm SST regime is obviously confined to low latitudes where free tropospheric temperature has little spatial and temporal variations on a seasonal time scale. As a result, EIS is approximately a function of SST only. The scatter plot of red open markers shows that EISs are negatively correlated with SSTs in most subtropical LSC regions, i.e., the Peruvian, Namibian, and Canary Islands regions, where early studies indicated the negative correlation between SST and the LSC amount (e.g., Hanson 1991; Oreopoulos and Davies 1993; Weare 1994). However, the negative correlation between EIS and SST is rather unclear in the Californian region; it is suggested that EIS around this region is more controlled by free tropospheric temperature than SST (KH93; Kubar et al. 2012).

On the other hand, in the cold SST regime, free tropospheric temperature rapidly decreases poleward and has large seasonal variations as well as SST. Thus, EIS is not determined only by SST. The scatter plot of blue filled markers indicates no correlation between SST and EIS in the midlatitude LSC regions defined by KH93. In addition, it is found that a transitional area between warm and cold SST regimes can be seen in the SST range of approximately 16–20°C, where the variance of EIS is maximum; the seasonal variation in the Australian LSC region is similar to those in the midlatitude regions.

Norris and Klein (2000) have shown that Sc is associated with divergence and subsidence, whereas St and FOG are associated with slight convergence and ascent, from observational composites at a midlatitude ocean weather station. Although not shown, we also note that we briefly analyzed the distribution of the 700-hPa pressure vertical velocity (ω_{700}) from ERA-40 in this SST–EIS field; results for the 500- and 850-hPa levels are quite similar. In the warm SST regime, the mean ω_{700} values are positive except for the domain where EISs are negative and SSTs are greater than 26°C, obviously corresponding to the tropical convective regions, and they tend to increase with EIS. This suggests that increases in EIS and the Sc amount in this regime are associated with large-scale subsidence, as reported by many previous studies. On the other hand, the mean ω_{700} values are near neutral or weak negative in the cold SST regime, although both the correlations with EIS and LSC-type amounts shown in the upper panels of Fig. 3 are poor. The general difference in sign of vertical motion is consistent with the dominant occurrence of Sc in the warm SST regime and the occurrence of all three types of LSCs in the cold SST regime.

3.2 Relationships between the LSC-type amounts and EISs for divided layers

EIS can be defined as a measure of inversion strength at any level between the 700-hPa level and the surface. In the previous subsection, an increase in EIS is associated with amounts of different LSC types between the warm and cold SST regimes. The result suggests that increases in EIS in the two regimes correspond to those in the inversion strength at different levels, because, as

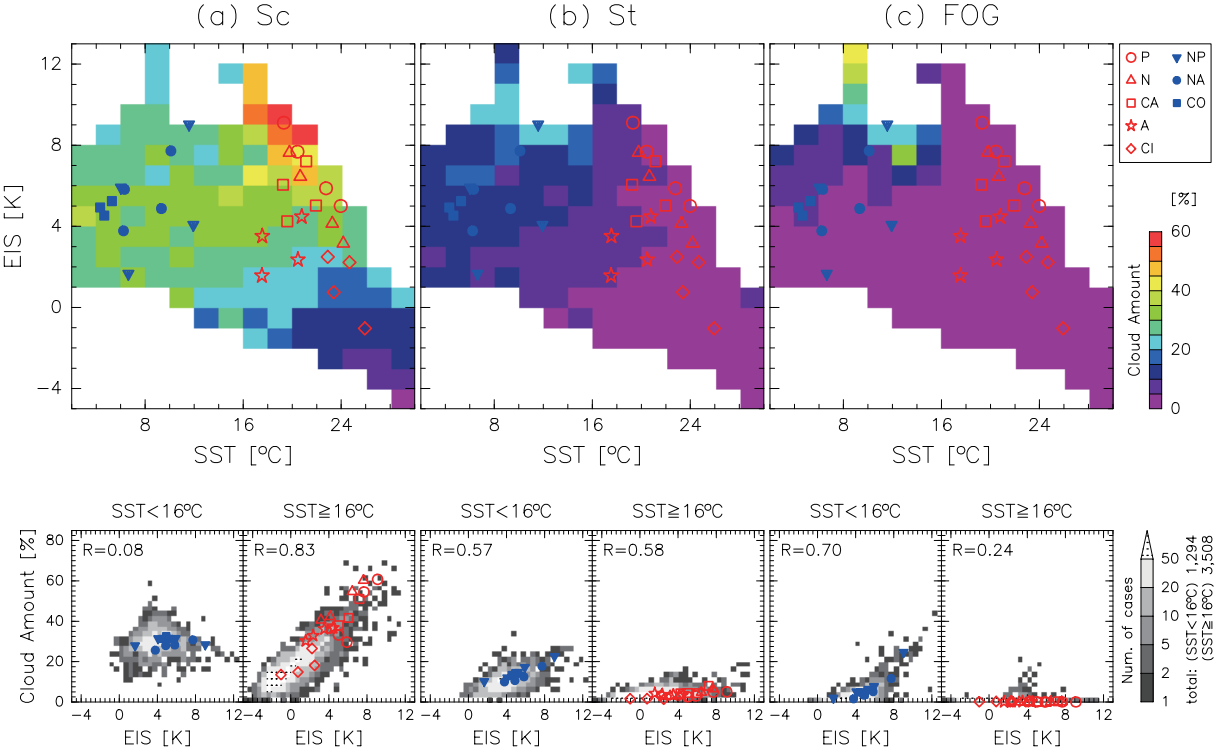

Fig. 3. (top) Mean (a) Sc, (b) St, and (c) FOG amounts for SST and EIS intervals for all 5° × 5° seasonal climatologies. Markers represent scatter plots of EIS with SST seasonally averaged for LSC regions defined by KH93 (Table 1); red open and blue filled markers correspond to those in the subtropical and midlatitude oceans, respectively. (bottom) As in Fig. 2 but for each LSC-type amount in the warm SST regime (SST ≥ 16°C) and the cold SST regime (SST < 16°C).

mentioned in the introduction, some previous studies from field campaigns or ocean weather station observations revealed that Sc, St, and FOG occur with inversions at different heights consistent with their morphologies (e.g., Norris 1998a). This would not be expected as a matter of course, because the definitions of these LSC types have no concrete information about differences in cloud-top heights.

To consider the vertical levels in which temperature inversion contributing to EIS exists within the framework of WB06, we introduce EISs for three layers between the 700-hPa level and the surface:

$$\mathrm{EIS} = \mathrm{EIS}_{850}^{700} + \mathrm{EIS}_{925}^{850} + \mathrm{EIS}_{\mathrm{sfc}}^{925}, \tag{2}$$

where

$$\mathrm{EIS}_{850}^{700} = (\theta_{700} - \theta_{850}) - \Gamma_{\mathrm{m}}^{850}(z_{700} - z_{850}) \tag{3}$$

is EIS for the layer between 700- and 850-hPa levels,

$$\mathrm{EIS}_{925}^{850} = (\theta_{850} - \theta_{925}) - \Gamma_{\mathrm{m}}^{850}(z_{850} - z_{925}) \tag{4}$$

is EIS for the layer between 850- and 925-hPa levels, and

$$\mathrm{EIS}_{\mathrm{sfc}}^{925} = (\theta_{925} - \theta_{\mathrm{sfc}}) - \Gamma_{\mathrm{m}}^{850}(z_{925} - z_{\mathrm{LCL}}) \tag{5}$$

is EIS for the layer between 925-hPa level and the surface. θ_{850} and θ_{925} are the potential temperatures at 850- and 925-hPa levels, respectively. Furthermore, z_{850} and z_{925} are the heights of the 850- and 925-hPa levels, respectively, which are calculated from equations similar to that for z_{700} described in WB06. The 5° × 5° seasonal climatologies of EISs for the three layers were calculated using the 2.5° × 2.5° monthly means of ERA-40 for the ocean grid points. If z_{LCL} exceeds z_{925}, EIS_{925}^{850} and $\mathrm{EIS}_{\mathrm{sfc}}^{925}$ were calculated as $(\theta_{850} - \theta_{925}) - \Gamma_{\mathrm{m}}^{850}(z_{850} - z_{\mathrm{LCL}})$ and $\theta_{925} - \theta_{\mathrm{sfc}}$, respectively; however, it was extremely rare in this calculation.

Figure 4 compares the global distributions of the LSC-type amounts with those of EISs for the divided layers for the JJA climatologies, with an SST of 16°C, which is a criterion separating the warm and cold SST regimes. Although we only show the JJA climatolo-

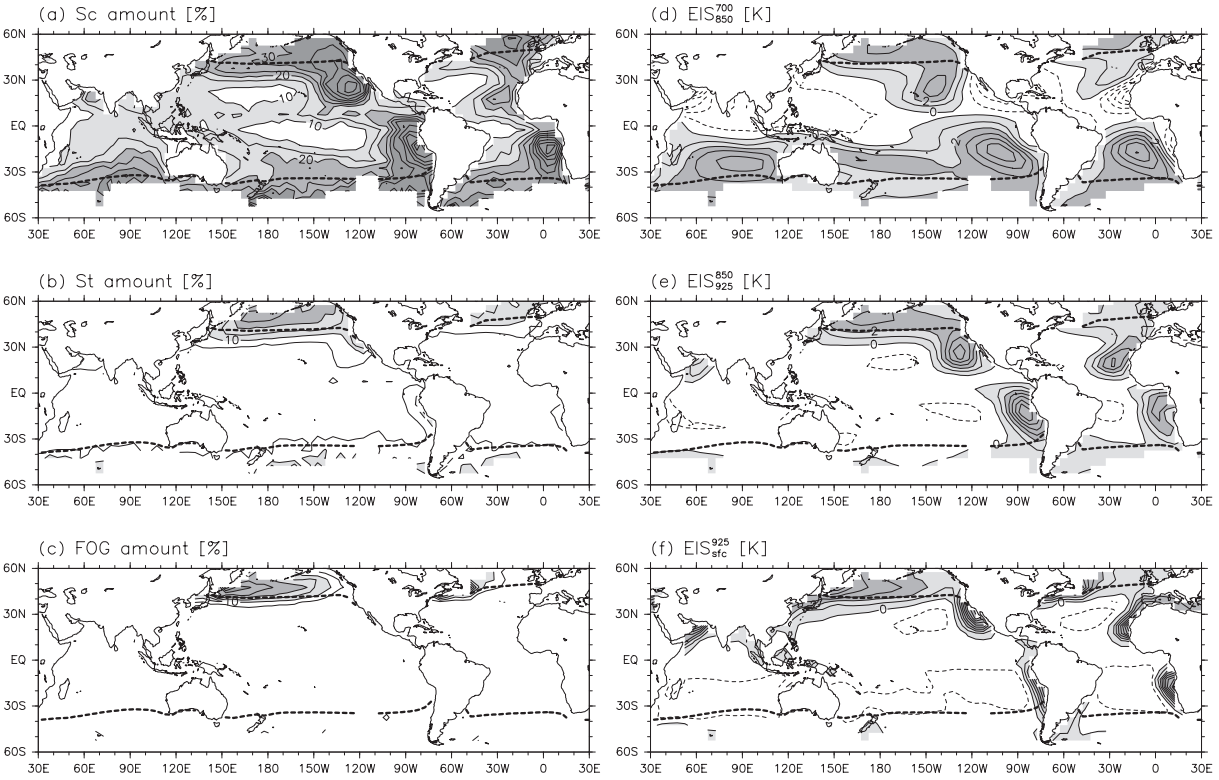

Fig. 4. (left) Climatological mean (a) Sc, (b) St, and (c) FOG amounts for the JJA season. Contour interval is 5%. Values greater than 10%, 20%, and 30% are shaded light gray, gray, and dark gray, respectively. (right) Climatological mean (d) EIS^{700}_{850}, (e) EIS^{850}_{925}, and (f) EIS^{925}_{sfc} for the JJA season. Contour interval is 1 K. Values greater than 0 K are lightly shaded and values greater than 2 K are heavily shaded. Dashed line indicates an SST of 16°C.

gies because the peaks in the annual cycle of the LSC amount occur during this season in most LSC regions defined by KH93 (highest seasons in the Peruvian and Namibian regions and in the Australian region are from JJA to SON and in DJF, respectively), the correspondences of distributions between the LSC-type amounts and EISs for the divided layers that will be described here are generally observed throughout the year. In addition, the climatological distributions of LSC-type amounts (Figs. 4a–c) have essentially been demonstrated in Norris (1998b); although he showed the frequency-of-occurrence instead of the average cloud amount, they are not very different because most variations in the average cloud amount are due to frequency-of-occurrence and amount-when-present is globally more uniform.

As shown in Figs. 4d–f, in the warm SST regime (equatorward of 16°C SSTs), high values of EISs for divided layers are concentrated in the subtropical eastern Pacific and Atlantic basins; however, the locations of the maxima shift westward in the order of EIS^{925}_{sfc}, EIS^{850}_{925}, and EIS^{700}_{850}. This indicates that inversion heights become deeper from east to west. Maxima in EIS^{700}_{850} also occur over the subtropical southern Indian Ocean. On the other hand, in the cold SST regime (poleward of 16°C SSTs), high values of EISs for divided layers are generally observed, although the distributions in the Southern Ocean are rather unclear in JJA due to insufficient numbers of ship-based observations. The east–west contrast is most prominent in the distribution of EIS^{925}_{sfc}: the maxima occur in the northwest Pacific and Atlantic.

Regarding the comparison with LSC-type amounts, the correspondence of distributions is different between warm and cold SST regimes. The global distributions of Sc amount (Fig. 4a) closely match those of EIS^{850}_{925} (Fig. 4e) in the warm SST regime. Hu et al. (2008) indicated that low cloud amount observed from satellites around KH93's Namibian LSC region is well correlated with the vertical temperature gradient between 850- and 925-hPa levels, while the correlation is weak with that between 700- and 850-hPa levels.

Table 2. Correlation coefficients between the LSC-type amounts and EISs for the divided layers and as a whole in the warm and cold SST regimes. The parentheses indicate that the correlation coefficient is not statistically significant at the 99% confidence level.

LSC type	SST ≥ 16°C				SST < 16°C			
	EIS_{850}^{700}	EIS_{925}^{850}	EIS_{sfc}^{925}	EIS	EIS_{850}^{700}	EIS_{925}^{850}	EIS_{sfc}^{925}	EIS
Sc	0.51	0.80	(0.04)	0.83	0.42	0.17	–0.31	0.08
St	0.25	0.48	0.26	0.58	0.34	0.56	0.32	0.57
FOG	(0.03)	0.13	0.27	0.24	0.16	0.63	0.66	0.70

Moreover, Kawai and Teixeira (2010) showed that over the subtropical eastern Pacific, meteorological factors related to the stability between 850- and 1000-hPa levels have higher correlations with the amount and other properties of LSCs compared to LTS and EIS. Their results are consistent with ours for much larger ocean areas. In the cold SST regime, the Sc amounts are somewhat larger than expected from the corresponding EIS_{925}^{850} values, compared with those in the warm SST regime. Although high values of EIS_{850}^{700} occur where the Sc amounts are larger especially in the southern hemisphere (Fig. 4d), the correspondence of distributions is rather weak. As mentioned in Fig. 3, the subtropical southern Indian Ocean including the Australian LSC region seems to be a transitional area between the warm and cold SST regimes; although SSTs in this domain are greater rather than 16°C, the Sc amount tends to be associated with EIS_{850}^{700} rather than EIS_{925}^{850}.

On the other hand, FOG amount (Fig. 4c) and EIS_{sfc}^{925} (Fig. 4f) in the cold SST regime are in good agreement on the large-scale distribution. In the warm SST regime, FOG rarely occurs; however, high EIS_{sfc}^{925} values occur in the coastal areas near KH93's subtropical LSC regions, as well as in the Arabian Sea. These areas correspond to those with relatively large St amounts in the subtropical oceans, although the sensitivity of the St amount to EIS_{sfc}^{925} is very low (Fig. 4b). A reason for the low sensitivity is that "no-low-cloud" ($C_L = 0$) is also frequently reported as a low cloud condition in these areas; the occurrence of no-low-cloud coincides with a strong surface stratification with less low-level moisture, and it might be associated with warm advection of dry air from land (Norris 1998a, b). In the cold SST regime, large St amounts coincide with relatively high values of EIS_{850}^{700}, EIS_{925}^{850}, and EIS_{sfc}^{925}. This is consistent with the result from the observation at a midlatitude ocean weather station that St often occurs with a moderate stable condition throughout MBL (Norris 1998a).

For the warm and cold SST regimes, Table 2 lists the correlation coefficients of LSC-type amounts with EIS for each divided layer as well as with EIS. The strong correlation of Sc amount with EIS_{925}^{850} coincides with a strong correlation with EIS in the warm SST regime. In the cold SST regime, the Sc amount is rather weakly but positively correlated with EIS_{850}^{700} and negatively correlated with EIS_{sfc}^{925}, even though no correlation can be observed with EIS. In contrast, the correlation of FOG amounts in the cold SST regime is higher with lower layer EISs; the correlation coefficient with EIS_{sfc}^{925} is highest and closest to that with EIS. Although there is no strong correlation between St amounts and EISs for any divided layer in both SST regimes, relatively high correlations are observed with EIS_{925}^{850}, especially in the cold SST regime. These results indicate that EISs for the divided layers appear to capture well the corresponding LSC-type amounts in the two regimes in spite of the coarse vertical resolution of ERA-40 for detecting the detailed changes in the potential temperature with height. However, it is also noted that EISs for the divided layers are comparable but not better predictors than EIS, except for the Sc amount in the cold SST regime, compared with the correlation coefficients also shown in the lower panels of Fig. 3.

3.3 Responses of LSC-type amounts and EISs for divided layers to EIS and their relationship to temperature advection

Figure 5 summarizes the average variations in the LSC-type amounts and EISs for divided layers with increasing EIS. To examine the association of advection over the ocean, the average air–sea temperature difference is also displayed, along with SST and the 2-m temperature. In the warm SST regime (Fig. 5a), an increase in EIS coincides well with increases in EIS_{925}^{850} and the Sc amount, corresponding to a decrease in SST as shown in Fig. 3. This result indicates that capping inversion strength around 1 km dominantly contributes to EIS and is associated with the Sc amount. As reviewed in Wood (2012), it is known that the devel-

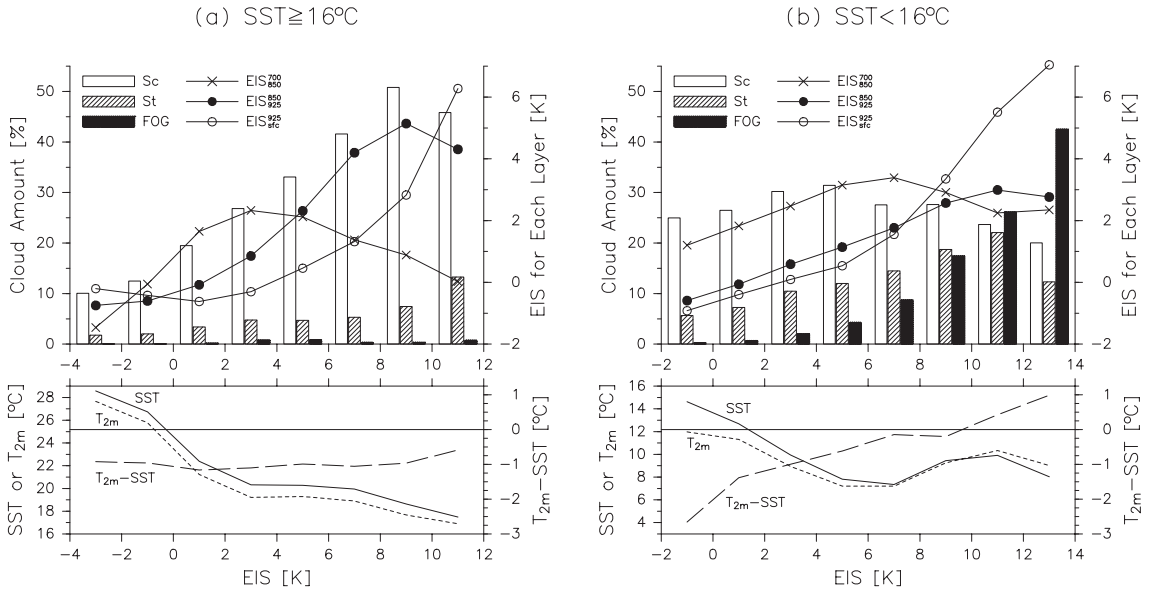

Fig. 5. (top) LSC-type (Sc, St, and FOG) amounts and EISs for three divided layers in the lower troposphere (EIS^{700}_{850}, EIS^{850}_{925}, and EIS^{925}_{sfc}) averaged into intervals of EIS in the (a) warm and (b) cold SST regimes. (bottom) SST (solid), 2-m temperature (dotted), and air–sea temperature difference (dashed) averaged into intervals of EIS in the (a) warm and (b) cold SST regimes.

opment and maintenance of Sc are closely linked with those of a capping inversion by longwave radiative cooling at the Sc top. In addition, these variations are associated with large-scale subsidence, as mentioned in the previous subsection.

On the other hand, the air–sea temperature differences are negative regardless of EIS, approximately –1°C; this implies that cold advection generally occurs in this regime. The resulting surface fluxes of heat and moisture from the ocean to the atmosphere are favorable for forming Sc. The variations in EISs for the divided layers also indicate that the dominant layer contributing to EIS changes in the order of EIS^{700}_{850}, EIS^{850}_{925}, and EIS^{925}_{sfc} as EIS increases. This suggests that an increase in EIS corresponds to a decrease in the average height of capping inversion; in the subtropical eastern oceans, the temperature inversion increases in height toward the west, as shown in Figs. 4d–f, accompanied by the transition from a relatively shallow, well-mixed MBL topped by Sc to a deeper decoupled MBL with trade cumulus (e.g., Albrecht et al. 1995b; Yuter et al. 2000; Garreaud et al. 2001). Such variations in temperature and cloud structure are associated with cold advection due to trade winds (Klein et al. 1995; Klein 1997; Xu et al. 2005; Mansbach and Norris 2007).

With the EIS maxima greater than 10 K, EIS^{925}_{sfc} surpasses the slightly decreasing EIS^{850}_{925}. This high value of EIS^{925}_{sfc} suggests a very shallow mixed layer, corresponding to the relatively large St amount of over 10% and the slightly decreasing Sc amount, as also shown in Fig. 3. They occur in the coastal areas near KH93's subtropical LSC regions (Figs. 4b, f).

In the cold SST regime (Fig. 5b), the variations in EIS^{700}_{850}, EIS^{850}_{925}, and EIS^{925}_{sfc} with increasing EIS are in good agreement with those in Sc, St, and FOG amounts, respectively. Relatively large values (20%–30%) of the Sc amount generally correspond to those of EIS^{700}_{850} around 2 K. This suggests that Sc in the cold SST regime exists at higher levels than in the warm SST regime. Recent satellite radar measurements also displayed a roughly uniform Sc field with a top height of approximately 2 km over the Southern Ocean (Huang et al. 2012). Moreover, in the range where EISs are less than approximately 8 K, all EISs for the divided layers increase at comparable rates. This implies that the entire lower troposphere gradually becomes stable. All three LSC-type amounts tend to weakly increase in this range. The gradual increase in EIS^{850}_{925} continues with that in the St amount in the range where EISs are higher; however, EIS^{925}_{sfc} rapidly increases exceeding EIS^{700}_{850} and EIS^{850}_{925}. This corresponds to an increase in FOG amount up to over 40%, although the frequencies are lower, as mentioned in Fig. 1. On the other hand, EIS^{700}_{850} and the Sc amount tend to decrease. EIS^{850}_{925}

and the St amount also decrease in the maximum EIS range.

With these variations, the air–sea temperature difference increases from negative to positive values, suggesting the transition from cold to warm advection over the ocean. The warm advection often leads to a surface-based inversion, which is reflected in the increase in EIS_{sfc}^{925}, due to cooling of warm air by heat transfer to the cold ocean; if the air is sufficiently moist, the cooling causes it to reach saturation and FOG forms (Norris and Klein 2000; Tokinaga and Xie 2009). In addition, the meridional SST gradient is generally strong in the cold SST regime. Therefore, the LSC type is highly sensitive to synoptic wind direction associated with extratropical cyclones in the storm track: Sc or St for equatorward cold advection, and FOG for poleward warm advection (Norris and Iacobellis 2005; Tanimoto et al. 2009). This may be why the Sc and St amounts are not very small for seasonal mean warm advection.

4. Conclusions

Using ship-based cloud observational data from EECRA and atmospheric reanalyses from ERA-40, we have investigated the seasonal relationship of the amounts of Sc, St, and FOG, of which LSCs consist, with EIS over the global ocean. Two different relationships for each LSC type are observed between the cloud amounts and EIS, corresponding to the variations for the subtropical and midlatitude LSC regions defined by KH93. This latitudinal difference is physically expected to relate closely to SST, because it primarily decreases with increasing latitude and plays an essential role in regulating the temperature and moisture structures in the lower troposphere. We have therefore examined the difference in the relationships between the LSC-type amounts and EIS by SST. It is found that the relationships are clearly divided into two regimes at an SST of approximately 16°C.

Sc is the only dominant type and its amount is strongly correlated with EIS in the warm SST regime, whereas the St and FOG amounts increase with EIS in the cold SST regime. This suggests that given the same EIS in both warm and cold SST regimes, the inferred inversion contributing to EIS exists at a different level for each SST regime. To consider the vertical difference within the framework of WB06, we introduced EISs for three layers between the 700-hPa level and the surface: EIS_{850}^{700}, EIS_{925}^{850}, and EIS_{sfc}^{925}. Although the vertical resolution of ERA-40 is too coarse for detecting the detailed changes in the potential temperature with height, EISs for the three layers are sufficient to distinguish among the associated inversion levels with Sc, St, and FOG.

The present study clearly revealed the responses of the LSC-type amounts and EISs for divided layers to increasing EIS. The Sc amount and EIS_{925}^{850} increase with EIS in the warm SST regime. In the cold SST regime, relatively large values of the Sc amount and EIS_{850}^{700} are exceeded by a rapid increase in FOG and EIS_{sfc}^{925}, while the St amount and EIS_{925}^{850} slightly increase with EIS. Their relationships to temperature advection implied by the air–sea temperature difference are also distinctly different between the two regimes: general occurrence of cold advection provides the favorable condition to form Sc and capping inversion in the warm SST regime, whereas warm advection causes an increase in the surface-based inversion strength in the cold SST regime, leading to more FOG.

These results indicate the importance of cloud types for identifying processes responsible for variations in the LSC amount. In particular, the importance should be emphasized in the cold SST regime, because LSCs are not dominated by a single type. Based on the relationships with the LSC-type amounts from the ship-based observations, EISs for divided layers can help diagnose the type of LSC amount observed by satellites or simulated by climate models. Although the target areas are limited by the number of ship-based observations, further investigation is required to examine the long-term variations of relationships between the LSC-type amounts and related processes such as those considered in this study.

Acknowledgments

The authors wish to thank Youichi Tanimoto and Shang-Ping Xie for helpful discussions throughout this work. Thanks are also extended to Yoko Naito and Hideaki Kawai for their valuable suggestions. The authors are grateful to two anonymous reviewers for providing insightful comments. Constructive criticism from three other anonymous reviewers has helped improve an early version of the manuscript. The EECRA data were obtained from the Carbon Dioxide Information Analysis Center, Oak Ridge National Laboratory, U.S. Department of Energy (http://cdiac.ornl.gov/epubs/ndp/ndp026c/ndp026c.html). The ERA-40 data were provided by the ECMWF Data Server (http://data-portal.ecmwf.int/). The HadISST data were taken from the official website (http://www.metoffice.gov.uk/hadobs/hadisst/). Data analysis and visualization were performed using the GFD-Dennou Ruby libraries.

References

Albrecht, B. A., C. S. Bretherton, D. Johnson, W. H. Scubert, and A. S. Frisch, 1995a: The Atlantic Stratocumulus Transition Experiment-ASTEX. *Bull. Amer. Meteor. Soc.*, **76**, 889–904.

Albrecht, B. A., M. P. Jensen, and W. J. Syrett, 1995b: Marine boundary layer structure and fractional cloudiness. *J. Geophys. Res.*, **100**, 14209–14222.

Albrecht, B. A., D. A. Randall, and S. Nicholls, 1988: Observations of marine stratocumulus clouds during FIRE. *Bull. Amer. Meteor. Soc.*, **69**, 618–626.

Bolton, D., 1980: The computation of equivalent potential temperature. *Mon. Wea. Rev.*, **108**, 1046–1053.

Bretherton, C. S., E. Klinker, A. K. Betts, and J. A. Coakley Jr., 1995: Comparison of ceilometer, satellite, and synoptic measurements of boundary-layer cloudiness and the ECMWF diagnostic cloud parameterization scheme during ASTEX. *J. Atmos. Sci.*, **52**, 2736–2751.

Bretherton, C. S., T. Uttal, C. W. Fairall, S. E. Yuter, R. A. Weller, D. Baumgardner, K. Comstock, R. Wood, and G. B. Raga, 2004: The EPIC 2001 stratocumulus study. *Bull. Amer. Meteor. Soc.*, **85**, 967–977.

Bretherton, C. S., R. Wood, R. C. George, D. Leon, G. Allen, and X. Zheng, 2010: Southeast Pacific stratocumulus clouds, precipitation and boundary layer structure sampled along 20°S during VOCALS-REx. *Atmos. Chem. Phys.*, **10**, 10639–10654.

Eastman, R., S. G. Warren, and C. J. Hahn, 2011: Variations in cloud cover and cloud types over the ocean from surface observations, 1954–2008. *J. Climate*, **24**, 5914–5934.

Garreaud, R. D., J. Rutllant, J. Quintana, J. Carrasco, and P. Minnis, 2001: CIMAR-5: A snapshot of the lower troposphere over the subtropical southeast Pacific. *Bull. Amer. Meteor. Soc.*, **82**, 2193–2207.

George, R. C., and R. Wood, 2010: Subseasonal variability of low cloud radiative properties over the southeast Pacific Ocean. *Atmos. Chem. Phys.*, **10**, 4047–4063.

Hahn, C. J., W. B. Rossow, and S. G. Warren, 2001: ISCCP cloud properties associated with standard cloud types identified in individual surface observations. *J. Climate*, **14**, 11–28.

Hahn, C. J., and S. G. Warren, 2009: *Extended edited synoptic cloud reports from ships and land stations over the globe, 1952–1996 (2009 update)*. CDIAC Numerical Data Package, NDP-026C, 79 pp.

Hahn, C. J., S. G. Warren, and J. London, 1995: The effect of moonlight on observation of cloud cover at night, and application to cloud climatology. *J. Climate*, **8**, 1429–1446.

Hanson, H. P., 1991: Marine stratocumulus climatologies. *Int. J. Climatol.*, **11**, 147–164.

Harrison, E. F., P. Minnis, B. R. Barkstrom, V. Ramanathan, R. D. Cess, and G. G. Gibson, 1990: Seasonal variation of cloud radiative forcing derived from the Earth Radiation Budget Experiment. *J. Geophys. Res.*, **95**, 18687–18703.

Hartmann, D. L., M. E. Ockert-Bell, and M. L. Michelsen, 1992: The effect of cloud type on earth's energy balance: Global analysis. *J. Climate*, **5**, 1281–1304.

Hu, Z.-Z., B. Huang, and K. Pegion, 2008: Low cloud errors over the south-eastern Atlantic in the NCEP CFS and their association with lower-tropospheric stability and air-sea interaction. *J. Geophys. Res.*, **113**, D12114, doi:10.1029/2007JD009514.

Huang, Y., S. T. Siems, M. J. Manton, L. B. Hande, and J. M. Haynes, 2012: The structure of low-altitude clouds over the Southern Ocean as seen by CloudSat. *J. Climate*, **25**, 2535–2546.

Jensen, M. P., A. M. Vogelmann, W. D. Collins, G. J. Zhang, and E. P. Luke, 2008: Investigation of regional and seasonal variations in marine boundary layer cloud properties from MODIS observations. *J. Climate*, **21**, 4955–4973.

Kawai, H., and J. Teixeira, 2010: Probability density functions of liquid water path and cloud amount of marine boundary layer clouds: Geographical and seasonal variations and controlling meteorological factors. *J. Climate*, **23**, 2079–2092.

Klein, S. A., 1997: Synoptic variability of low-cloud properties and meteorological parameters in the subtropical trade wind boundary layer. *J. Climate*, **10**, 2018–2039.

Klein, S. A., and D. L. Hartmann, 1993: The seasonal cycle of low stratiform clouds. *J. Climate*, **6**, 1587–1606.

Klein, S. A., D. L. Hartmann, and J. R. Norris, 1995: On the relationships among low-cloud structure, sea surface temperature, and atmospheric circulation in the summertime northeast Pacific. *J. Climate*, **8**, 1140–1155.

Kubar, T. L., D. E. Waliser, J.-L. Li, and X. Jiang, 2012: On the annual cycle, variability, and correlations of oceanic low-topped clouds with large-scale circulation using Aqua MODIS and ERA-Interim. *J. Climate*, **25**, 6152–6174.

Lenschow, D. H., I. R. Paluch, A. R. Bandy, R. Pearson Jr., S. R. Kawa, C. J. Weaver, B. J. Huebert, J. G. Kay, D. C. Thornton, and A. R. Driedger III, 1988: Dynamics and Chemistry of Marine Stratocumulus (DYCOMS) experiment. *Bull. Amer. Meteor. Soc.*, **69**, 1058–1067.

Lin, W., M. Zhang, and N. G. Loeb, 2009: Seasonal variation of the physical properties of marine boundary layer clouds off the California coast. *J. Climate*, **22**, 2624–2638.

Mansbach, D. K., and J. R. Norris, 2007: Low-level cloud variability over the equatorial cold tongue in observations and models. *J. Climate*, **20**, 1555–1570.

Minnis, P., P. W. Heck, D. F. Young, C. W. Fairall, and J. B. Snider, 1992: Stratocumulus cloud properties derived from simultaneous satellite and island-based instrumentation during FIRE. *J. Appl. Meteor.*, **31**, 317–339.

Norris, J. R., 1998a: Low cloud type over the ocean from

surface observations. Part I: Relationship to surface meteorology and the vertical distribution of temperature and moisture. *J. Climate*, **11**, 369–382.

Norris, J. R., 1998b: Low cloud type over the ocean from surface observations. Part II: Geographical and seasonal variations. *J. Climate*, **11**, 383–403.

Norris, J. R., and S. F. Iacobellis, 2005: North Pacific cloud feedbacks inferred from synoptic-scale dynamic and thermodynamic relationships. *J. Climate*, **18**, 4862–4878.

Norris, J. R., and S. A. Klein, 2000: Low cloud type over the ocean from surface observations. Part III: Relationship to vertical motion and the regional surface synoptic environment. *J. Climate*, **13**, 245–256.

Norris, J. R., and C. B. Leovy, 1994: Interannual variability in stratiform cloudiness and sea surface temperature. *J. Climate*, **7**, 1915–1925.

O'Dell, C. W., F. J. Wentz, and R. Bennartz, 2008: Cloud liquid water path from satellite-based passive microwave observations: A new climatology over the global oceans. *J. Climate*, **21**, 1721–1739.

Oreopoulos, L., and R. Davies, 1993: Statistical dependence of albedo and cloud cover on sea surface temperature for two tropical marine stratocumulus regions. *J. Climate*, **6**, 2434–2447.

Park, S., and C. B. Leovy, 2004: Marine low-cloud anomalies associated with ENSO. *J. Climate*, **17**, 3448–3469.

Ramanathan, V., R. D. Cess, E. F. Harrison, P. Minnis, B. R. Barkstrom, E. Ahmad, and D. Hartmann, 1989: Cloud-radiative forcing and climate: Results from the Earth Radiation Budget Experiment. *Science*, **243**, 57–63.

Rayner, N. A., D. E. Parker, E. B. Horton, C. K. Folland, L. V. Alexander, D. P. Rowell, E. C. Kent, and A. Kaplan, 2003: Global analyses of sea surface temperature, sea ice, and night marine air temperature since the late nineteenth century. *J. Geophys. Res.*, **108**, 4407, doi:10.1029/2002JD002670.

Rossow, W. B., and R. A. Schiffer, 1999: Advances in understanding clouds from ISCCP. *Bull. Amer. Meteor. Soc.*, **80**, 2261–2287.

Rozendaal, M. A., C. B. Leovy, and S. A. Klein, 1995: An observational study of diurnal variations of marine stratiform cloud. *J. Climate*, **8**, 1795–1809.

Sassen, K., and Z. Wang, 2008: Classifying clouds around the globe with the CloudSat radar: 1-year of results. *Geophys. Res. Lett.*, **35**, L04805, doi:10.1029/2007GL032591.

Stevens, B., D. H. Lenschow, G. Vali, H. Gerber, A. Bandy, B. Blomquist, J.-L. Brenguier, C. S. Bretherton, F. Burnet, T. Campos, S. Chai, I. Faloona, D. Friesen, S. Haimov, K. Laursen, D. K. Lilly, S. M. Loehrer, S. P. Malinowski, B. Morley, M. D. Petters, D. C. Rogers, L. Russell, V. Savic-Jovcic, J. R. Snider, D. Straub, M. J. Szumowski, H. Takagi, D. C. Thornton, M. Tschudi, C. Twohy, M. Wetzel, and M. C. van Zanten, 2003: Dynamics and Chemistry of Marine Stratocumulus—DYCOMS-II. *Bull. Amer. Meteor. Soc.*, **84**, 579–593.

Tanimoto, Y., S.-P. Xie, K. Kai, H. Okajima, H. Tokinaga, T. Murayama, M. Nonaka, and H. Nakamura, 2009: Observations of marine atmospheric boundary layer transitions across the summer Kuroshio Extension. *J. Climate*, **22**, 1360–1374.

Tokinaga, H., and S.-P. Xie, 2009: Ocean tidal cooling effect on summer sea fog over the Okhotsk Sea. *J. Geophys. Res.*, **114**, D14102, doi:10.1029/2008JD011477.

Uppala, S. M., P. W. Kållberg, A. J. Simmons, U. Andrae, V. da Costa Bechtold, M. Fiorino, J. K. Gibson, J. Haseler, A. Hernandez, G. A. Kelly, X. Li, K. Onogi, S. Saarinen, N. Sokka, R. P. Allan, E. Andersson, K. Arpe, M. A. Balmaseda, A. C. M. Beljaars, L. van de Berg, J. Bidlot, N. Bormann, S. Caires, F. Chevallier, A. Dethof, M. Dragosavac, M. Fisher, M. Fuentes, S. Hagemann, E. Hólm, B. J. Hoskins, L. Isaksen, P. A. E. M. Janssen, R. Jenne, A. P. McNally, J.-F. Mahfouf, J.-J. Morcrette, N. A. Rayner, R. W. Saunders, P. Simon, A. Sterl, K. E. Trenberth, A. Untch, D. Vasiljevic, P. Viterbo, and J. Woollen, 2005: The ERA-40 re-analysis. *Quart. J. Roy. Meteor. Soc.*, **131**, 2961–3012.

Warren, S. G., C. J. Hahn, J. London, R. M. Chervin, and R. L. Jenne, 1986: *Global distribution of total cloud cover and cloud type amounts over land*. NCAR Technical Note, NCAR/TN-273+STR, 29 pp.

Warren, S. G., C. J. Hahn, J. London, R. M. Chervin, and R. L. Jenne, 1988: *Global distribution of total cloud cover and cloud type amounts over the ocean*. NCAR Technical Note, NCAR/TN-317+STR, 42 pp.

Weare, B. C., 1994: Interrelationships between cloud properties and sea surface temperatures on seasonal and interannual time scales. *J. Climate*, **7**, 248–260.

Weare, B. C., 1999: Combined satellite- and surface-based observations of clouds. *J. Climate*, **12**, 897–913.

Weare, B. C., 2000: Near-global observations of low clouds. *J. Climate*, **13**, 1255–1268.

Wood, R., 2012: Stratocumulus clouds. *Mon. Wea. Rev.*, **140**, 2373–2423.

Wood, R., and C. S. Bretherton, 2006: On the relationship between stratiform low cloud cover and lower-tropospheric stability. *J. Climate*, **19**, 6425–6432.

Wood, R., C. S. Bretherton, and D. L. Hartmann, 2002: Diurnal cycle of liquid water path over the subtropical and tropical oceans. *Geophys. Res. Lett.*, **29**, 2092, doi:10.1029/2002GL015371.

Woodruff, S. D., H. F. Diaz, J. D. Elms, and S. J. Worley, 1998: COADS Release 2 data and metadata enhancements for improvements of marine surface flux fields. *Phys. Chem. Earth*, **23**, 517–526.

Woodruff, S. D., R. J. Slutz, R. L. Jenne, and P. M. Steurer, 1987: A Comprehensive Ocean-Atmosphere Data Set. *Bull. Amer. Meteor. Soc.*, **68**, 1239–1250.

World Meteorological Organization, 1975: *International Cloud Atlas. Volume I: Manual on the Observation of Clouds and Other Meteors*. WMO-No. 407, WMO, Geneva, Switzerland, 155 pp.

World Meteorological Organization, 1995: *Manual on Codes. Volume I.1: Part A: Alphanumeric codes*. WMO-No. 306, WMO, Geneva, Switzerland, 462 pp.

Xu, H., S.-P. Xie, and Y. Wang, 2005: Subseasonal variability of the southeast Pacific stratus cloud deck. *J. Climate*, **18**, 131–142.

Yue, Q., B. H. Kahn, E. J. Fetzer, and J. Teixeira, 2011: Relationship between marine boundary layer clouds and lower tropospheric stability observed by AIRS, CloudSat, and CALIOP. *J. Geophys. Res.*, **116**, D18212, doi:10.1029/2011JD016136.

Yuter, S. E., Y. L. Serra, and R. A. Houze Jr., 2000: The 1997 Pan American Climate Studies Tropical Eastern Pacific Process Study. Part II: Stratocumulus region. *Bull. Amer. Meteor. Soc.*, **81**, 483–490.

Zhang, Y., B. Stevens, B. Medeiros, and M. Ghil, 2009: Low-cloud fraction, lower-tropospheric stability, and large-scale divergence. *J. Climate*, **22**, 4827–4844.

Zuidema, P., and D. L. Hartmann, 1995: Satellite determination of stratus cloud microphysical properties. *J. Climate*, **8**, 1638–1657.